Unexpected Chemical Activity of a Mineral Surface: The Role of Crystal Water in Tobermorite

Mohammadreza Izadifar, Carsten Natzeck, Katja Emmerich, Peter G. Weidler, Soheil Gohari, Colin Burvill, and Peter Thissen*

ABSTRACT: The most prominent phase of hydrated cement paste, as a model for calcium silicate hydrate (CSH) gel, is tobermorite with varying Ca/Si ratios. In the present work, carbon monoxide (CO) gas is introduced onto the surface of tobermorite at 62 K. The experimental results from infrared spectroscopy reveal a chemical reaction of CO with tobermorite, leading to the formation of carbonate (CO_3^{2-}), which is adsorbed on the surface. This chemical reaction is driven by the dissociation of crystal water incorporated in the tobermorite structure. In infrared spectroscopy, the saturation of this carbonate growth process is revealed by the adsorption of unreacted CO molecules sticking to the surface of the fresh $CaCO_3$. Interestingly, the decomposition process performed by heating the system leads to CO_2 emission rather than CO. Our results are underlined by density functional theory calculations that bring out the high significance of interlayer water.

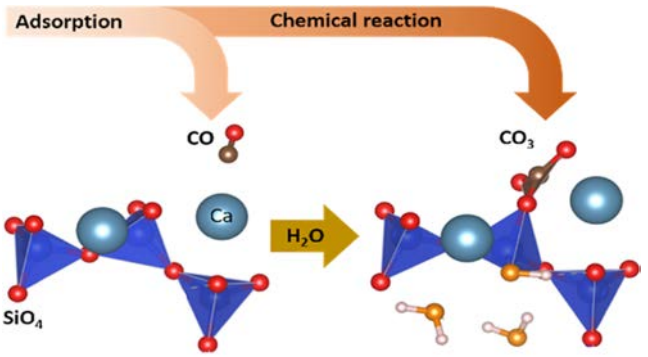

1. INTRODUCTION

Calcium silicate hydrate (CSH) gel[1−3] is a significant component of concrete, which encompasses 60−70% of the fully hydrated cement paste and is responsible for the mechanical properties of cementitious materials. CSH gel is mostly recognized by the proportion of calcium to silicon in the range from 0.7 to 2.3.[4] The most prominent phases of hydrated cement paste as a model for CSH gel are tobermorite 14,[5,6] 11,[6−8] and 9[6,9] Å with different Ca/Si ratios.[1,3] 14 Å tobermorite ($Ca_5Si_6O_{16}(OH)_2{\cdot}7H_2O$) is the most hydrous one. In other words, three different degrees of hydration depending on the amount of interlayer water can influence the distance between two consecutive chains of the silicate tetrahedra, resulting in the formation of three different tobermorites.[10] The most common structure of natural tobermorite under ambient conditions is tobermorite 11 Å ($Ca_5Si_6O_{17}{\cdot}5H_2O$), which can exist in two different polymorphs called normal and anomalous. The most significant difference between them is that while the normal tobermorite transforms into tobermorite 9 Å ($Ca_5Si_6O_{17}$) upon heating, the anomalous tobermorite keeps its characteristic spacing at 11 Å in spite of the loss of the interlayer water.[7] Tobermorite minerals have also been found to be beneficial in industrial applications of hazardous wastewater treatment and cation exchange.[11−14] As a model of CSH gel, the major hydrated phase of cement, the tobermorite surface chemistry is substantial in comprehension of the cement structure and its interaction with fluids and ions.[15]

The interaction of aqueous solutions with mineral surfaces is one of the most important chemical reactions in nature. Such reactions play a major role in the dissolution, precipitation, and sorption processes. They also influence the composition and quality of natural waters, soil formation, the removal of CO_2 from the atmosphere, the uptake and release of plant nutrients, the mobility of heavy metal pollutants, and the global cycle of chemical elements. They could also be responsible for the binding of water on Mars and the formation of prebiotic molecules at the beginning of the earth's history. Interfacial reactions between solid surfaces and aqueous solutions are also important in the production and performance of metal-on-metal oxide catalysts, metal corrosion and surface passivation, the cleaning of semiconductor surfaces, chemical sensors, and water treatment. Historically, these processes were thought to only occur at wet interfaces in the earth's crust,[16] and the reaction rates can increase with low concentrations of aqueous solutions at the interface.[17] Putnis et al.[18] reported that

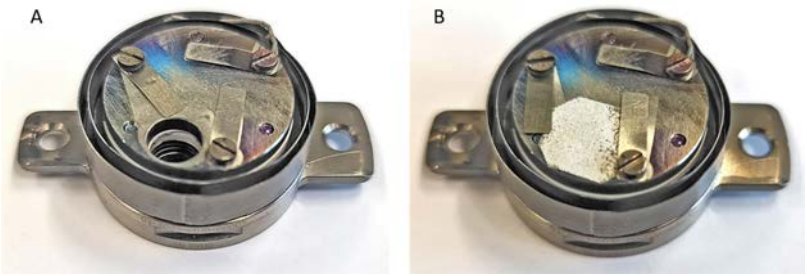

Figure 1. (A) Photograph of a sample holder designed for UHV infrared measurement in transmission mode. The diameter of the hole is 10 mm. (B) Photograph of a tobermorite powder sample, pressed in a mesh and mounted on the holder.

dissolution, and consequently, recrystallization at the mineral interface are dependent on the fluid interfaces. The interaction of water is indeed of particular interest for mineral interfaces. Detailed spectroscopic investigations under ultra-high vacuum (UHV) conditions and calculations based on density functional theory (DFT) on the interaction of water with a well-defined mineral substrate are largely lacking.

An increase in knowledge about the chemical and physical behavior of the surfaces in cement-bound materials and their components is thus of particular importance for improving the performance of these important materials. To observe the $CaCO_3$ formation on the surface of minerals without interlayer water, we[19] performed a study of CO at wollastonite(001). On the dry surface of wollastonite(001), the CO adsorbs as a monolayer at 62 K. After one monolayer has formed, the reaction comes to a standstill. Another study was performed to prove the effect of water at the interface of minerals with CO_2 absorbents. Longo et al.[20] confirmed that a carbonate monolayer is formed, but further reactions stop at the water-free interface of wollastonite(001) with CO_2. They also proved that the mechanism of carbonation is strongly affected and completely changed in the presence of water for the adsorption of CO_2 on wollastonite in the ambient atmosphere. This is due to the metal−proton exchange reaction (MPER) via the removal of Ca^{2+} ions from the surface and transferring them to the $CaCO_3$ formation site. Therefore, either water from the ambient atmosphere or the mineral interface can accelerate the $CaCO_3$ formation.

Modern infrared spectroscopy makes use of probe molecules to investigate new effects in surface science. In this context, one of the most popular probe molecules is CO. In UHV and at temperatures around 80 K, CO can be adsorbed and reveals useful information about the surface structure. Due to its linear geometric and electronic structure, CO has universal utility. The CO gas phase frequency is found at 2143 cm^{-1}. Most commonly, CO forms surface carbonyl complexes with metal atoms and metal ions. Materials of interest in heterogeneous catalysis, construction chemistry, and biology are polycrystalline solids forming polydisperse surface species. Surface termination may result in the exposure of several crystal planes or several surface species simultaneously and usually differs from the ideal bulk structure due to surface defects, reconstruction, and adsorption from the environment. Consequently, surface arrangements cannot be deduced in a straightforward mannner from the bulk structure, which complicates the identification of active sites. Adsorption of probe molecules combined with different spectroscopic methods gives information about the nature of surface sites. Retrievable information has been shown to be the type and number of sites, the chemical and electronic surface properties of sites, the relative abundance, and the site distribution. In this context, specific interaction with certain sites and sufficient sensitivity with respect to the differences in the electronic structure of various surface sites are major features of probe molecules.

In this work, we demonstrate the significant role of interlayer water at mineral interfaces. While CO adsorbs as a monolayer on wollastonite without any chemical reaction and desorbs again in the form of CO, it completely reacts with the surface of tobermorite. With the help of DFT, we found one possible chemical reaction pathway explaining the dissociation of interlayer water incorporated in tobermorite as a driving force.

2. METHODS

2.1. Materials. Tobermorite granular material was commercially acquired (SIMPur, Cirkel, Deutschland). Granules were finely ground in an agate mortar prior to XRD and STA measurements. For infrared experiments in UHV, granules were ground in the protective gas atmosphere in a glovebox and directly transferred to the UHV sample chamber.

Preparation and transfer of tobermorite powder to the XRD and STA machine without contact with the atmosphere were impossible. Thus, the prepared tobermorite powder has reacted partially with gases from the atmosphere (including carbon monoxide).

2.2. X-ray Diffraction (XRD). XRD measurements were performed on a Bruker D8 Advance instrument in the Bragg−Brentano geometry (θ−θ setup) together with a PSD Lynxeye-XE (192 Si-strips) detector. Measurements were performed with a step size of 0.01° 2θ and a scan speed of 2 s/step (resulting in a total time of 384 s per step due to the PSD) in a range of 5° < 2θ < 80° with Cu Kα (λ = 1.54186 Å) radiation. The diffractograms were evaluated with the Bruker DIFFRAC.EVA 5.2 software; the estimation of the quantitative composition and determination of the mean coherence length (MCL, similar to crystallite sizes) were done via the Rietveld method as implemented in the Bruker AXS TOPAS6.0 program.

2.3. Simultaneous Thermal Analysis (STA). The measurements were performed on an STA 449 C Jupiter (Netzsch-Gerätebau GmbH, Selb, Germany) equipped with a thermogravimetry/differential scanning calorimetry (TG/DSC) sample holder. The STA was connected to a quadrupole mass spectrometer (MS) 403 C Aëolos (InProcess Instruments (IPI)/NETZSCH-Gerätebau GmbH, Selb, Germany) by a heated quartz glass capillary (T = 230 °C). Masses m/z = 16, 18, 28, and 44 were monitored. Samples were heated at 10 K/min from 35 to 1000 °C in 50 mL/min flowing Ar that was mixed with 20 mL/min Ar from the protective gas flow. Pt/Rh crucibles (diameter 5 mm and height 5 mm) with a punched

lid were filled with 100 mg of material. An empty Pt/Rh crucible with a lid served as an inert reference sample. The dynamic heating segment was preceded by an isothermal segment at 35 °C for 10 min to equilibrate the furnace atmosphere.

2.4. Fourier Transform Infrared (FTIR) Spectroscopy. All infrared experiments were performed in a multi-technique ultrahigh vacuum (UHV) apparatus (Prevac, Poland). A more comprehensive description of the experimental setup can be found elsewhere.[21] First, 4-5 mg of the tobermorite powder was weighted. This material was pressed in a steel mesh (GoodFellow, Rostfreieer Stahl–Werkstoff Nr. 1.4401 (Fe/Cr_{18}/Ni_{10}/Mo_3) mesh) with a pressure of 6-7 tons and for 2 min. The preparation of the sample was performed inside a glovebox to have clean surfaces. A photograph of the sample holder with a prepared sample holder is shown in Figure 1. The thickness of the pressed sample holder could be approximated at 0.1 mm. After the sample holder was introduced onto the UHV system, it was first measured for 72 h at room temperature to gas out. The infrared data was acquired using infrared light with a normal incidence angle (90°) and a spectral resolution of 1 cm^{-1}. The base pressure of the UHV chamber amounted to 4.0×10^{-11} mbar. Dosing of CO was performed using a capillary tube ending in front of the sample with the temperature of the sample held at 62 K. The temperature of the samples was monitored by a K-type thermocouple that was attached to the edge of the sample holder. An exposure of one milli-Langmuir (mL) corresponds to 1.33×10^{-9} mbar·s.

2.5. Density Functional Theory (DFT). We examined the interactions between the interface of tobermorite 11 Å (004) and CO within density functional theory[22] using electronic structure calculations. The Vienna Ab initio Simulation Package (VASP)[23−26] with the projected-augmented wave (PAW) method was used to define electron-ion interaction. A well-converged plane–wave cutoff energy of 400 eV was employed. The electron exchange and correlation functional was chosen in the generalized gradient approximation (GGA) with the Perdew–Burke–Ernzerhof (PBE) parametrization.[27] A force tolerance of 0.01 eV $Å^{-1}$ was applied for structural optimizations. The Brillouin zone was sampled using a well-converged *k*-sampling equivalent given by 3 × 3 × 1 Monkhorst–Pack *k*-points for the total system.[28] The optimized primitive unit cell of tobermorite 11 Å was characterized by the following parameters: a = 6.73 Å, b = 7.37 Å, c = 22.68 Å and $\alpha = \beta = 90°$, $\gamma = 123.18°$ (we refer to the monoclinic system with spacegroup #8 B11m, called normal tobermorite, $Ca_5Si_6O_{17}·5H_2O$).[7] Then, a model of tobermorite 11 Å (004)[15] was developed with periodic boundary conditions along x and y directions to remove the finite length effects, and a vacuum slab with an approximate thickness of 7 Å between the 004 surface and the adjacent cell was considered to avoid the interactions in the z direction. The contribution of van der Waals (vdW) interaction for all configurations in this study was neglected.

3. RESULTS AND DISCUSSION

XRD was performed to characterize the tobermorite powder. XRD is a swift analytical technique employed for identification of unknown phases of crystalline materials and can provide information on unit cell dimensions. The results, shown in Figure 2, demonstrate that the employed tobermorite powder is dominated by tobermorite 11 Å with a content of 5

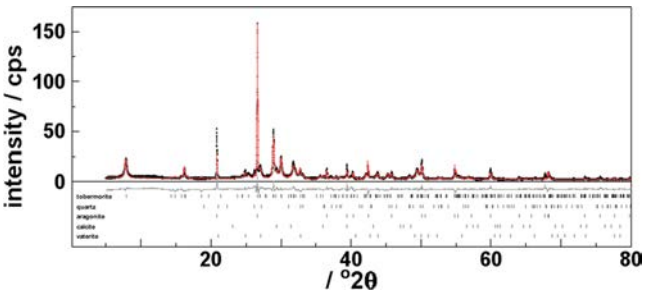

Figure 2. XRD patterns of the synthetic tobermorite powder. + represents the raw data, colored line the resultant fit, and gray line the difference curve (data-fit); the vertical bars mark the peak position of the respective mineral phase used in the fit.

interlayer water molecules per unit cell. Two different models for the tobermorite were tested for the Rietveld refinement: one setting in the orthorhombic system with spacegroup #43 Fdd2 and the other in the monoclinic system with spacegroup #8 B11m.[7] The refinement performed better with the monoclinic model than with the orthorhombic model. Thus, tobermorite resembles normal tobermorite, as described by Merlino et al.[7] Models for quartz, vaterite, aragonite and calcite were obtained from the Crystallography Open Database,[29] which were all present in minor quantities in the sample. The Rietveld refinement revealed that the dominating phase was tobermorite with 58 ± 4 wt %, followed by vaterite 16 ± 2 wt %, quartz 14 ± 1 wt %, aragonite 8 ± 1 wt %, and calcite 6 ± 4 wt %.

The DSC, coupled with MS, shows different peaks associated with the emission of H_2O or CO_2. The first peak in the range of 20–400 °C is commonly related to dehydration, as well as to the emission of physically bound water. It is very easy to detect the DTG/MS peak related to the dehydroxylation around 550 °C. Beyond this temperature range, the decarbonation of $CaCO_3$ is observed with a pronounced emission of CO_2 detected by MS even if residual water can still be emitted between 500 and 700 °C. The decomposition of $CaCO_3$ is characterized by the presence of three DSC/MS peaks (see Figure 3). Above 800 °C, the material starts to decompose into thermodynamically more stable phases. Most commonly, these are wollastonite and quartz.

The peak in the MS line m/z 28 at 300 °C, which is declared as carbon monoxide, was unexpected and has so far not been reported in the literature. For the measurements in STA, we used tobermorite powder before it was used in the UHV/IR measurements. The reason is that one measurement of STA needs 100 mg of the tobermorite powder (which cannot be used in other experiments afterward), while an experiment with the UHV-holder just needs 4–5 mg of the material. Additionally, transferring to the STA machine without contact with the atmosphere would be impossible. Thus, the prepared tobermorite powder has reacted partially with gases from the atmosphere (including carbon monoxide).

The reaction of carbon monoxide with tobermorite shown in this study can be described in the following steps:

$$CO^{gas} + Ca_5Si_6O_{17}·5H_2O \rightleftharpoons CO_3Ca_5Si_6O_{14}(OH)_2·4H_2O$$

(62 K, −211.15 °C)

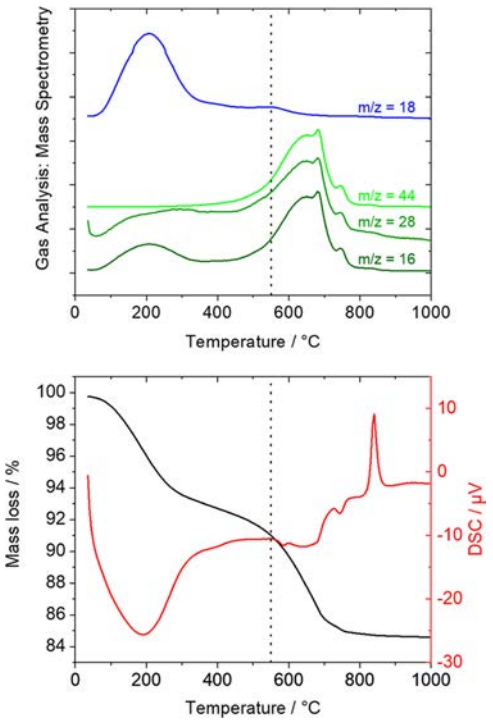

Figure 3. Thermogravimetric analysis with complementary gas phase analysis of the tobermorite powder. The mass loss of H_2O (m/z = 18) related to tobermorite decomposition usually occurs in the range of 50−550 °C. The desorption of molecular water (dehydration) took place from room temperature to 220 °C. At 300 °C, a peak in the line m/z 28 (carbon monoxide) can be found. Around 550 °C, surface hydroxyl groups recombine to water and desorb (dehydroxylation). The escape of CO_2 (m/z = 44) from $CaCO_3$ resulting from carbonation can start just after the dehydroxylation peak (550−600 °C) and is generally prolonged until 900−950 °C.

$$CO_3Ca_5Si_6O_{14}(OH)_2 \cdot 4H_2O \rightleftharpoons CO_3Ca_5Si6O_{14}(OH)_2 + 4\,(H_2O)^{gas} \quad (200\ °C)$$

$$CO_3Ca_5Si_6O_{14}(OH)_2 \rightleftharpoons Ca_5Si_6O_{16}(OH)_2 + CO^{gas} \quad (300\ °C)$$

$$CO_3Ca_5Si_6O_{14}(OH)_2 \rightleftharpoons CO_3Ca_5Si_6O_{14} + H_2O^{gas} \quad (550\ °C)$$

$$CO_3Ca_5Si_6O_{14} \rightleftharpoons Ca_5Si_6O_{15} + CO_2{}^{gas} \quad (>550\ °C)$$

The mechanism described here is not catalytic. In contrast to the materials investigated so far, a covalently bound carbonate−silicate[30] is formed in these reactions, and high temperatures are necessary to detach this species from the surface again. To validate our observations and precisely understand the mechanism of CO_3 decomposition at a higher temperature, Giraudo et al. studied the dehydroxylation of CSH phases.[36] They investigated materials with a Ca/Si ratio of less than one, like tobermorite, and after heating those materials, the final products were quartz and wollastonite with Ca/Si equal to 0 and 1, respectively. Moreover, it has also been reported that after 600 °C, carbonate converts to CO_2 and is completely removed.

In the next part of this study, we report that CO deposition at the interface of tobermorite results in the formation of CO_3, which is dependent on the dissociation of the interlayer water of the mineral. In contrast, we remind the readers that according to previous studies carried out in UHV conditions, CO adsorbs and forms a monolayer on the surface.[31−33] Stibor et al. also reported the half and a quarter monolayer CO coverage for the adsorption of CO on the clean metal cluster of an Fe(110) surface through the DFT calculation method.[34] Another computational study, performed for a monolayer of CO adsorption on Fe_3O_4 at various coverages within the DFT calculation method by Yu et al.,[35] reported that more than one CO could adsorb on one surface ion atom on both Fe_{tet1} and Fe_{oct2} terminations of Fe_3O_4(111). Therefore, our results associated with CO adsorption on a mineral surface in the present study completely disclose different in comparison to the former investigations. Initially, we placed tobermorite powder in the UHV conditions to ensure the dry interface. After the sample holder was introduced into the UHV system, infrared measurements were performed for 72 h at room temperature to gas out the prepared sample. Results are shown in Figure 4.

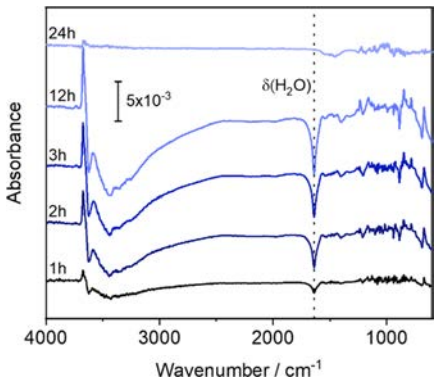

Figure 4. Time-dependent infrared spectra were measured after the sample holder with the prepared tobermorite was introduced into the UHV system. Spectra are referred to the previous time as the baseline (1−24 h).

The HOH bending vibration of molecular water at 1653 cm^{-1} can directly be associated with the loss of water contained in the pores of the powder of the prepared powder sample. A quantitative prediction of the number of water molecules in the pore volume could be made with the help of the Kelvin equation. The OH stretching vibration depicts one continuous part from 3800 to 2500 cm^{-1}, which is correlated to the molecular water of the pores. When this water desorbs, the OH-groups and water molecules remaining in the system have to reorient. This can lead to a change in the dipole moment and a dispersive shape in the infrared spectra. The vibrations below 1300 cm^{-1} can all be associated with the silicate tetrahedral chains of the tobermorite running along the [010] axis. When the water desorbs, these chains have to reorient.

After a stable baseline in infrared was reached, the sample was cooled down to 62 K. Different doses of carbon monoxide were then injected into the system at the interface of tobermorite. Surprisingly, we found a barrier-less chemical reaction of carbon monoxide with tobermorite resulting in interlayer water dissociation and $CaCO_3$ formation. Therefore, IR spectra of different doses of CO molecules (10, 100, 1000,

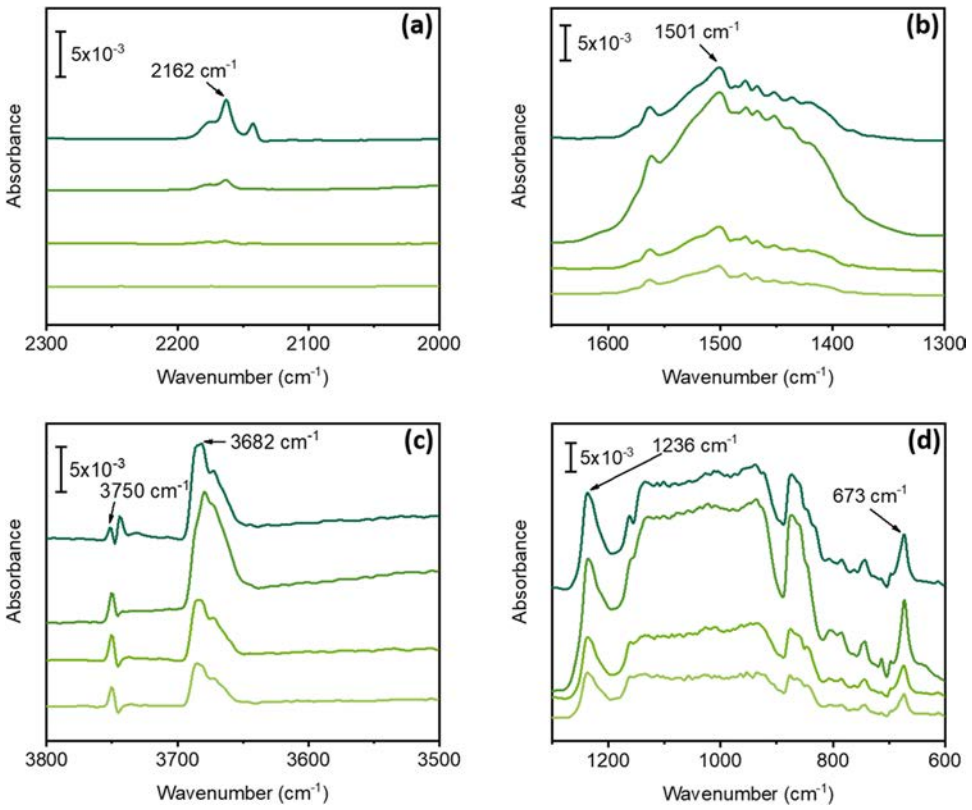

Figure 5. IR spectra of the adsorption of different doses of CO molecules on the surface of tobermorite 11 Å. (a-d) Classified IR spectra including 2300-2000, 1650-1300, 3800-3500, and 1300-600 cm^{-1}, respectively. Light to dark green colors for the IR spectra represent the different doses of CO (10, 100, 1000, 10000 mL), respectively. Note that the spectra are referred to the previous dose of CO.

10 000 mL) on the surface of tobermorite are shown in Figure 5.

Figure 5a,b illustrates the significant peaks for the two stretching vibrations of ν(C−O) and $\nu_{as}(CO_3)$ at 2162 and 1501 cm^{-1}, respectively.[19,36] The $\nu_{as}(CO_3)$ on the surface of tobermorite at 1501 cm^{-1} is shown by an incremental trend for peak intensity as the injection of CO increases from 10 to 1000 mL. By 10 000 mL of CO dosing, the growth of CO_3 slows down due to sufficient accumulation of CO_3 on the surface of tobermorite and instead the peak of CO appears at 2162 cm^{-1} for the CO molecule adsorption on the tobermorite surface. In Figure 5c,d, together with the sequential dissociation of the water molecules and the peak intensities corresponing to the stretching vibrations of ν(Ca−OH) and ν(Si−OH) at 3682 and 3750 cm^{-1} were increased by increasing the dosing of CO from 10 to 1000 mL. In contrast, by 10 000 mL of CO dosing, the interlayer water molecules were less dissociated, resulting in a decreasing trend at the absorbance of Ca−OH and Si−OH compared to 1000 mL; consequently, the growth of CO_3 on the surface of tobermorite slowed down. The peaks corresponding to the bending and stretching vibrations of δ(O−Si−O) and ν(Si−O) are seen at 673 and 1236 cm^{-1}, respectively.[36]

Figure 6 illustrates the peak intensities of the stretching vibrations of ν(CO) and $\nu_{as}(CO_3)$ at 2162 and 1501 cm^{-1} as a function of CO dosing, respectively. The peak intensity of the $\nu_{as}(CO_3)$ on the surface of tobermorite at 1501 cm^{-1} follows an incremental trend for the dosing of CO in the range of 10 to 1000 mL. At 10 000 mL of CO dosing, the growth of CO_3 slows down due to sufficient accumulation of CO_3 on the surface of tobermorite and instead the peak of ν(CO)

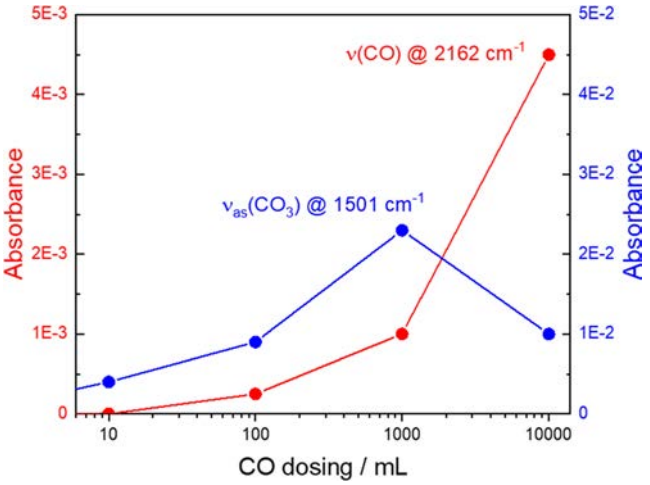

Figure 6. Absorbance intensity of the stretching vibrations of ν(CO) and $\nu_{as}(CO_3)$ at 2162 and 1501 cm^{-1} as a function of CO dosing. Note that the spectra in Figure 5 are referred to the previous dose of CO.

dominates at 2162 cm^{-1}. This peak could be compared to the ν(CO) on calcite(1.04), which was measured at 2164 cm^{-1}.[33] If there was a high amount of carbonate inside the sample, then the adsorption of CO on the carbonate would start from the beginning. However, as we have seen in XRD, there is a certain amount of carbonate inside the sample, but the tobermorite dominates. Otherwise, all effects like water dissociation, CO reaction, and CO adsorption, would not follow such a clear mechanism.

Next, we come back to the comparison of IR after saturation. The IR spectra of CO deposition on the clean surfaces of tobermorite and wollastonite in UHV conditions are shown in Figure 7. Obviously, a new vibrational peak appeared at 2162

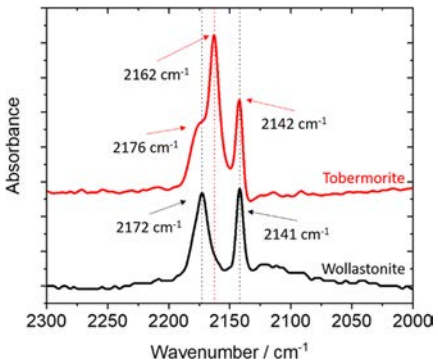

Figure 7. Comparison of infrared spectra of wollastonite and tobermorite. Both samples were prepared in a similar way: the powder was pressed on the steel mesh, put on the sample holder (Figure 1), introduced into UHV, and gassed out for 72 h. After cooling to 62 K, the samples were loaded with CO, and infrared spectra were measured (Figure 5). A clear difference can be seen in the peak at 2162 cm^{-1} (ν(CO) on carbonate), appearing only in the spectrum of the tobermorite.

cm^{-1} in tobermorite, also correlated to the CO, which is not seen in wollastonite.[37] This peak could be compared to the ν(CO) on calcite(1.04), which was measured at 2164 cm^{-1}.[33]

Infrared spectra of carbon monoxide adsorbed on metal oxides show mainly several distinct absorption bands. One has to keep in mind that calcium is the only metal on the surface and that it does not contain any d-electrons; consequently, we expect linear bonded carbon monoxides, and the shift in frequency can be associated with different surfaces. Lower frequencies can be correlated to a stronger binding to the surface, and therefore, the linear bonded carbon monoxide desorbs at a higher temperature. Carbon monoxide on calcite(1.04) desorbs at 100 K from the surface.[33] This would mean that the linear bonded carbon monoxide at 2176 cm^{-1} would desorb between 62 and 100 K and that the linear bonded carbon monoxide at 2142 cm^{-1} would desorb at a temperature higher than 100 K. From the discussion of TGA with gas monitoring, we see that this model is quite fitting.

According to the XRD measurement of tobermorite powder, we observed that the majority of measured tobermorite is from the type of 11 Å. In the following, to determine the proper interface for the tobermorite 11 Å with the carbon monoxide, the lowest surface energy for 004 according to the Miller index was computed to be 0.41 J/m^2 as reported by Mutisya et al.[15]

In Figure 8, the NEB method demonstrates a barrier-less reaction pathway of $CaCO_3$ formation through the reaction of CO on the surface of tobermorite 11 Å (004). To explain the NEB[38] reaction precisely, Figure 8 (point A) indicates the initial model of dreierketten silicate chain for deposition of CO at the tobermorite 11 Å (004) interface. Figure 8 (points B–D) displays the minima energy procedures of the system by approaching CO at the interface of tobermorite 11 Å. Figure 8 (point C) shows that CO_3 is not formed before the dissociation of interlayer water and it only bonded to one dangling oxygen coordinated to the silicon atom. The ground-state structure was obtained as the interlayer water dissociated, and therefore, the hydroxyl group was exchanged by the dangling oxygen from silicon to form 4-fold coordinated silicon and $CaCO_3$ formation on the surface of tobermorite (Figure 8, point D).

We investigated the changes in the electronic properties for deposition of CO due to $CaCO_3$ formation on the surface of tobermorite 11 Å (004). The charge density distribution for the initial and final simulations was obtained through NEB by Bader charge analysis, respectively. For the initial simulation, carbon had a total electron number of 2.9 at the valence band when it was situated far from the surface of tobermorite 11 Å (004). After $CaCO_3$ formation, carbon oxidized, and its total number of electrons decreased to 1.92. The total number of electrons each time in the system is constant, and oxidation of

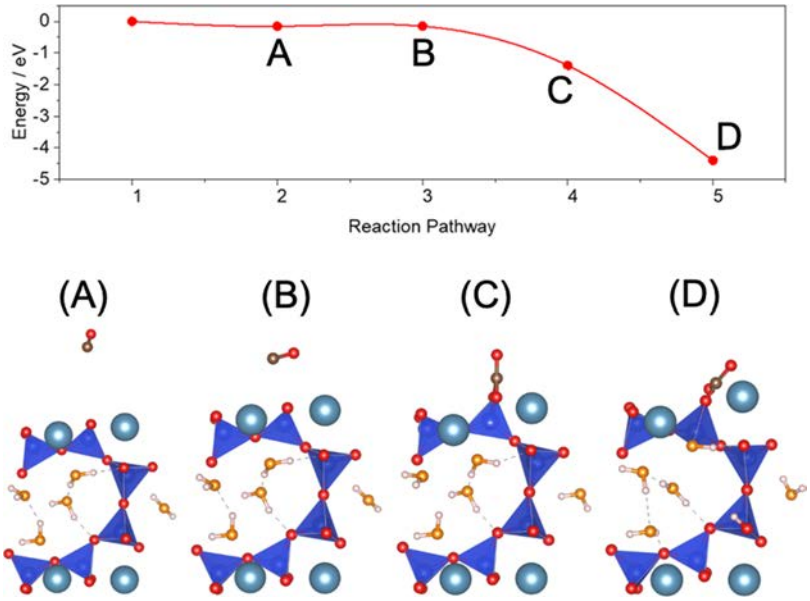

Figure 8. DFT calculation of the minimum energy path of CO reacting with the tobermorite 11 Å (004). The blue atoms represent Si; red O (yellow in the case of water); gray Ca; white H; and brown C atoms, respectively.

carbon leads to the reduction of other neighboring atoms (mainly the parts of the silicate chain, where the −OH groups form).

The water gas shift reaction (WGSR) describes the reaction of carbon monoxide and water vapor to form carbon dioxide and hydrogen.[39,40]

$$CO + H_2O \rightleftharpoons CO_2 + H_2$$

However, the family of CSH materials can be modified with the help of the so-called metal−proton exchange reaction (MPER)[41] and metal−metal exchange reaction (MMER), which may prove to be interesting in the future.[41] With these reactions, different metals have already been exchanged, and different properties in the CSH material have been changed.[41−43] Thus, the cheap CSH material could become even more interesting for the industry in the future.

4. CONCLUSIONS

In summary, we have investigated the surface structure and surface reactivity of normal tobermorite-11 by detecting the interaction of carbon monoxide with the help of infrared spectroscopy. FTIR measurement methods demonstrate that the growth of carbonate on the surface of tobermorite 11 Å occurs. This chemical reaction is driven by the dissociation of crystal water incorporated in the tobermorite structure. In infrared spectroscopy, the saturation of this carbonate growth process is revealed by the adsorption of unreacted CO molecules sticking to the surface of the fresh $CaCO_3$. These experiments have been performed at 62 K, which seems to be the lowest temperature reported for the formation of carbonate from carbon monoxide. Finally, we analyzed the carbonate decomposition process by STA with complementary gas phase analysis. The gas-phase monitoring results show carbon monoxide and carbon dioxide, but the origin in the decomposing material is not unambiguous.

AUTHOR INFORMATION

Corresponding Author

Peter Thissen − *Institute of Functional Interfaces (IFG), Karlsruhe Institute of Technology (KIT), 76344 Eggenstein-Leopoldshafen, Germany;* orcid.org/0000-0001-7072-4109; Email: peter.thissen@kit.edu

Authors

Mohammadreza Izadifar − *Institute of Construction and Building Materials, Technical University of Darmstadt, 64287 Darmstadt, Germany; Institute of Functional Interfaces (IFG), Karlsruhe Institute of Technology (KIT), 76344 Eggenstein-Leopoldshafen, Germany;* orcid.org/0000-0002-8153-4834

Carsten Natzeck − *Institute of Functional Interfaces (IFG), Karlsruhe Institute of Technology (KIT), 76344 Eggenstein-Leopoldshafen, Germany*

Katja Emmerich − *Competence Center for Material Moisture (IMB-CMM), Karlsruhe Institute of Technology (KIT), 76131 Karlsruhe, Germany;* orcid.org/0000-0001-5600-6581

Peter G. Weidler − *Institute of Functional Interfaces (IFG), Karlsruhe Institute of Technology (KIT), 76344 Eggenstein-Leopoldshafen, Germany*

Soheil Gohari − *Department of Mechanical Engineering, The University of Melbourne, Parkville, VIC 3010, Australia*

Colin Burvill − *Department of Mechanical Engineering, The University of Melbourne, Parkville, VIC 3010, Australia*

Notes

The authors declare no competing financial interest.

ACKNOWLEDGMENTS

The authors gratefully appreciate the financial support from the DFG. The authors highly acknowledge the fruitful discussions with Prof. Wöll. They also thank Nadja Werling for her assistance with TGA experiments that greatly improved the manuscript.

REFERENCES

(1) Taylor, H. F. W. Tobermorite, jennite, and cement gel. *Z. Kristallogr.* **1992**, *202*, 41−50.

(2) Izadifar, M.; Dolado, J. S.; Thissen, P.; Ayuela, A. Interactions between Reduced Graphene Oxide with Monomers of (Calcium) Silicate Hydrates: A First-Principles Study. *Nanomaterials* **2021**, *11*, 2248.

(3) Izadifar, M.; Königer, F.; Gerdes, A.; Wöll, C.; Thissen, P. Correlation between Composition and Mechanical Properties of Calcium Silicate Hydrates Identified by Infrared Spectroscopy and Density Functional Theory. *J. Phys. Chem. C* **2019**, *123*, 10868−10873.

(4) Dolado, J. S.; Griebel, M.; Hamaekers, J. A. Molecular Dynamic Study of Cementitious Calcium Silicate Hydrate (C−S−H) Gels. *J. Am. Ceram. Soc.* **2007**, *90*, 3938−3942.

(5) Bonaccorsi, E.; Merlino, S.; Kampf, A. R. The Crystal Structure of Tobermorite 14 Å (Plombierite), a C−S−H Phase. *J. Am. Ceram. Soc.* **2005**, *88*, 505−512.

(6) Richardson, I. G. The Calcium Silicate Hydrates. *Cem. Concr. Res.* **2008**, *38*, 137−158.

(7) Merlino, S.; Bonaccorsi, E.; Armbruster, T. The Real Structure of Tobermorite 11A: Normal and Anomalous Forms, OD Character and Polytypic Modifications. *Eur. J. Mineral.* **2001**, *13*, 577−590.

(8) Hamid, S. A. The Crystal Structure of the 11 Ä Natural Tobermorite $Ca_{2.25}[Si_3O_{7.5}(OH)_{1.5}].1H_2O$. *Z. Kristallogr. − Cryst. Mater.* **1981**, *154*, 189−198.

(9) Merlino, S.; Bonaccorsi, E.; Armbruster, T. The Real Structures of Clinotobermorite and Tobermorite 9 Å: OD Character, Polytypes, and Structural Relationships. *Eur. J. Mineral.* **2000**, *12*, 411−429.

(10) Diez-Garcia, M.; Gaitero, J. J.; Dolado, J. S.; Aymonier, C. Ultra-Fast Supercritical Hydrothermal Synthesis of Tobermorite under Thermodynamically Metastable Conditions. *Angew. Chem.* **2017**, *129*, 3210−3215.

(11) Shrivastava, O. P.; Shrivastava, R. Cation Exchange Applications of Synthetic Tobermorite for the Immobilization and Solidification of Cesium and Strontium in Cement Matrix. *Bull. Mater. Sci.* **2000**, *23*, 515−520.

(12) Li, L.; Wu, Z. X.; Li, Y. X.; Sha, H. L.; Song, G. W. Synthesis of Aluminum-Substituted Tobermorite and the Application on the Phosphorus Removal from Waste Water. *Desalin. Water Treat.* **2014**, *52*, 4292−4297.

(13) Kaneco, S.; Itoh, K.; Katsumata, H.; Suzuki, T.; Masuyama, K.; Funasaka, K.; Hatano, K.; Ohta, K. Removal of Natural Organic Polyelectrolytes by Adsorption on to Tobermorite. *Environ. Sci. Technol.* **2003**, *37*, 1448−1451.

(14) Komarneni, S.; Roy, D. M.Method of Storing Radioactive Wastes using Modified Tobermorite. U.S. Patent US4537710A, 1985.

(15) Mutisya, S. M.; Miranda, C. R. The Surface Stability and Morphology of Tobermorite 11 Å from First Principles. *Appl. Surf. Sci.* **2018**, *444*, 287−292.

(16) *Treatise on Geochemistry* Turekian, K.; Holland, H., Eds.; Elsevier: New York, 2014; Vol. *16*.

(17) Milke, R.; Neusser, G.; Kolzer, K.; Wunder, B. Very little Water is necessary to Make a Dry Solid Silicate System Wet. *Geology* **2013**, *41*, 247−250.
(18) Putnis, C. V. The Mineral−Water Interface: Where Minerals React with the Environment. *Elements* **2013**, *9*, 177−182.
(19) Thissen, P.; Natzeck, C.; Giraudo, N.; Weidler, P.; Wöll, C. Hydration of Concrete: The First Steps. *Chem. − Eur. J.* **2018**, *24*, 8603−8608.
(20) Longo, R. C.; Cho, K.; Bruner, P.; Welle, A.; Gerdes, A.; Thissen, P. Carbonation of Wollastonite(001) Competing Hydration: Microscopic Insights from Ion Spectroscopy and Density Functional Theory. *ACS Appl. Mater. Interfaces* **2015**, *7*, 4706−4712.
(21) Stammer, X.; Heißler, S. FTIR-Spektroskopie im Ultrahochvakuum: Messung an TiO_2-Pulver. *Nachr. Chem.* **2013**, *61*, 926−929.
(22) Kohn, W.; Sham, L. J. Self-Consistent Equations Including Exchange and Correlation Effects. *Phys. Rev.* **1965**, *140*, A1133−A1138.
(23) Kresse, G.; Hafner, J. Ab Initio Molecular Dynamics for Liquid Metals. *Phys. Rev. B* **1993**, *47*, 558−561.
(24) Kresse, G.; Furthmüller, J. Efficiency of Ab-Initio total Energy Calculations for Metals and Semiconductors using a Plane-Wave Basis Set. *Comput. Mater. Sci.* **1996**, *6*, 15−50.
(25) Kresse, G.; Furthmüller, J. Efficient Iterative Schemes for Ab Initio Total-Energy Calculations using a Plane-Wave Basis Set. *Phys. Rev. B* **1996**, *54*, 11169−11186.
(26) Izadifar, M.; Thissen, P.; Steudel, A.; Kleeberg, R.; Kaufhold, S.; Kaltenbach, J.; Schuhmann, R.; Dehn, F.; Emmerich, K. Comprehensive Examination of Dehydroxylation of Kaolinite, Disordered Kaolinite, and Dickite: Experimental Studies and Density Functional Theory. *Clays Clay Miner.* **2020**, *68*, 319−333.
(27) Perdew, J. P.; Burke, K.; Ernzerhof, M. Generalized Gradient Approximation Made Simple. *Phys. Rev. Lett.* **1996**, *77*, 3865−3868.
(28) Monkhorst, H. J.; Pack, J. D. Special Points for Brillouin-Zone Integrations. *Phys. Rev. B* **1976**, *13*, 5188−5192.
(29) Vaitkus, A.; Merkys, A.; Gražulis, S. Validation of the Crystallography Open Database using the Crystallographic Information Framework. *J. Appl. Crystallogr.* **2021**, *54*, 661−672.
(30) Santamaria-Perez, D.; Ruiz-Fuertes, J.; Pena-Alvarez, M.; Chulia-Jordan, R.; Marqueno, T.; Zimmer, D.; Gutierrez-Cano, V.; MacLeod, S.; Gregoryanz, E.; Popescu, C.; Rodriguez-Hernandez, P.; Munoz, A. Post-Tilleyite, a Dense Calcium Silicate-Carbonate Phase. *Sci. Rep.* **2019**, *9*, No. 7898.
(31) Vogt, J.; Vogt, B. The Structure of Carbon Monoxide Adsorbed on the NaCl(100) Surface—A Combined LEED and DFT-D/vdW-DF Study. *J. Chem. Phys.* **2014**, *141*, No. 214708.
(32) Eren, B.; Head, A. R. Carbon Monoxide Adsorption on Manganese Oxide/Cobalt: an Ambient Pressure X-Ray Photoelectron Spectroscopy Study. *J. Phys. Chem. C* **2020**, *124*, 3557−3563.
(33) Hafshejani, T. M.; Wang, W.; Heggemann, J.; Nefedov, A.; Heissler, S.; Wang, Y.; Rahe, P.; Thissen, P.; Wöll, C. CO Adsorption on the Calcite(10.4) Surface: a Combined Experimental and Theoretical Study. *Phys. Chem. Chem. Phys.* **2021**, *23*, 7696−7702.
(34) Stibor, A.; Kresse, G.; Eichler, A.; Hafner, J. Density Functional Study of the Adsorption of CO on Fe(110). *Surf. Sci.* **2002**, *507−510*, 99−102.
(35) Yu, X.; Zhang, X.; Jin, L.; Feng, G. CO Adsorption, Oxidation and Carbonate Formation Mechanisms on Fe_3O_4 Surfaces. *Phys. Chem. Chem. Phys.* **2017**, *19*, 17287−17299.
(36) Giraudo, N.; Thissen, P. Carbonation Competing Functionalization on Calcium-Silicate-Hydrates: Investigation of Four Promising Surface-Activation Techniques. *ACS Sustainable Chem. Eng.* **2016**, *4*, 3985−3994.
(37) Idriss, H.; Llorca, J. Low Temperature Infrared Study of Carbon Monoxide Adsorption on Rh/CeO_2. *Catalysts* **2019**, *9*, 598.
(38) Izadifar, M.; Ukrainczyk, N.; Salah Uddin, K. M.; Middendorf, B.; Koenders, E. Dissolution of Portlandite in Pure Water: Part 2 Atomistic Kinetic Monte Carlo (KMC) Approach. *Materials* **2022**, *15*, 1442.
(39) Gokhale, A. A.; Dumesic, J. A.; Mavrikakis, M. On the Mechanism of Low-Temperature Water Gas Shift Reaction on Copper. *J. Am. Chem. Soc.* **2008**, *130*, 1402−1414.
(40) Grabow, L. C.; Gokhale, A. A.; Evans, S. T.; Dumesic, J. A.; Mavrikakis, M. Mechanism of the Water Gas Shift Reaction on Pt: First Principles, Experiments, and Microkinetic Modeling. *J. Phys. Chem. C* **2008**, *112*, 4608−4617.
(41) Thissen, P. Exchange Reactions at Mineral Interfaces. *Langmuir* **2020**, *36*, 10293−10306.
(42) Longo, R. C.; Königer, F.; Nefedov, A.; Thissen, P. Chemical Properties of Metal-Silicates Rendered by Metal Exchange Reaction. *ACS Sustainable Chem. Eng.* **2019**, *7*, 8449−8457.
(43) Longo, R. C.; Schewe, N.; Weidler, P. G.; Heissler, S.; Thissen, P. Synthesis of Silicates for High-Performance Oxide Semiconductors: Electronic Structure Analysis. *ACS Appl. Electron. Mater.* **2021**, *3*, 299−308.